TRF1 uses a noncanonical function of TFIIH to promote telomere replication

Zhe Yang, Keshav Sharma, and Titia de Lange

Laboratory for Cell Biology and Genetics, Rockefeller University, New York, New York 10021, USA

Telomeric DNA challenges the replisome and requires TRF1 for efficient duplication. TRF1 recruits the BLM helicase, but BLM loss does not explain the extensive telomere fragility, ATR signaling, and sister telomere associations (STAs) induced by TRF1 deletion. Here, we document that Helix2 of the TRFH domain and Helix1 of the Myb domain of TRF1 are required for efficient telomere replication. Mutation of both helices generated a TRF1 separation-of-function mutant (TRF1-E83K/LW-TI) that induced severe telomere replication defects but no ATR signaling or STAs. We identified the transcription and nucleotide excision repair (NER) factor TFIIH as a critical effector of TRF1. Loss of TFIIH subunits, but no other NER factors, caused the same telomere replication phenotypes as the TRF1-E83K/LW-TI mutant independent of the effects on TRF1 expression. TFIIH subunits coimmunoprecipitated with wild-type TRF1 but not with TRF1-E83K/LW-TI. These results establish that the major mechanism by which TRF1 ensures telomere replication involves a noncanonical function of TFIIH.

Mammalian telomeres are bound by shelterin, which performs several key functions, including solving the end protection problem, maintaining and regulating telomere length, and facilitating telomere replication (Hockemeyer and Collins 2015; de Lange 2018). The TRF1 subunit of shelterin is crucial for the duplication of telomeres by the canonical DNA replication machinery. Deletion of TRF1 from mouse embryonic fibroblasts (MEFs) leads to replication fork stalling, ATR kinase activation in S phase, sister telomere associations (STAs), and a very prominent phenotype that is referred to as fragile telomeres because of its similarity to the cytogenetic appearance of common fragile sites (CFSs) (Martínez et al. 2009; Sfeir et al. 2009). Unlike the normal telomere fluorescent in situ hybridization (FISH) signals, which appear as discrete rounded entities at the end of each metaphase chromatid, fragile telomeres are elongated, decondensed, and/or broken up into multiple signals. Like CFSs, fragile telomeres are induced by a low dose of the polymerase α inhibitor aphidicolin, suggesting that they originate from defects in the replication of telomeric DNA (Sfeir et al. 2009).

One mechanism by which TRF1 facilitates telomere replication and prevents telomere fragility is through recruiting the BLM helicase to telomeres (Sfeir et al. 2009; Zimmermann et al. 2014). BLM is able to resolve G-quadruplex (G4) structures, which can be formed by the TTAGGG repeats that constitute the template for lagging strand DNA synthesis at telomeres. Loss of BLM leads to transient telomere-internal double-strand breaks (DSBs) that are generated by SLX4/SLX1 cleavage of single-stranded (ss) gaps and are repaired by break-induced replication (BIR) (Yang et al. 2020). The fragile telomere phenotype of BLM-deficient cells was shown to be due to this BIR (Yang et al. 2020). BIR-mediated fragile telomere formation is also observed in cells with artificially generated telomere-internal DSBs and in ALT (alternative lengthening of telomeres) cells, which harbor spontaneous telomere damage (Yang et al. 2020).

Whereas BLM deletion induces fragile lagging strand telomeres, BLM absence fails to explain all other phenotypes caused by TRF1 loss, including fragile leading strand telomeres, diminished telomere replication, ATR signaling, and STAs. Furthermore, the frequency of lagging strand fragile telomeres in BLM-deficient MEFs is lower than in TRF1-deficient cells (Sfeir et al. 2009; Zimmermann et al. 2014). Therefore, it is likely that TRF1 performs additional functions to promote the replication of the duplex telomeric repeat array.

Here, we report that telomere replication requires Helix2 of the TRFH domain and Helix1 of the Myb domain of TRF1. The contribution of Myb Helix1 to telomere replication was separate from its well-established role in telomeric DNA binding. Mutation of these two helices

yielded a TRF1 separation-of-function mutant (TRF1-E83K/LW-TI) that induced telomere replication defects on par with the phenotype of TRF1 deletion but retained the ability to localize to telomeres, repress ATR signaling, and prevent STAs. Unexpectedly, a CRISPR screen targeting candidate genes that might promote telomere replication identified TFIIH. TFIIH is a basal transcription factor that facilitates promoter opening through its XPB translocase, formation of the RNA polymerase II (PolII) preinitiation complex, and phosphorylation of the PolII CTD by its associated CDK-activating kinase (CAK, composed of CDK7, Cyclin H, and MNAT1) (Schier and Taatjes 2020). TFIIH is also required for the opening of the DNA duplex during nucleotide excision repair (NER), a repair pathway involving numerous XP factors in addition to the XPB translocase and XPD helicase in TFIIH (Compe and Egly 2016). Deletion of components of the TFIIH-CAK holoenzyme, but not NER factors XPA, XPC, XPF, and XPG, caused extensive fragile telomere formation and telomere replication defects but no other phenotypes of TRF1 loss. The role of TFIIH was independent of its effect on TRF1 expression. TFIIH was epistatic with TRF1, and several of its subunits bound to TRF1 but not to TRF1-E83K/LW-TI. These data reveal that TRF1 interacts with TFIIH and uses this complex to prevent telomere replication problems.

Results

Most fragile telomeres induced by TRF1 loss do not involve BLM, BIR, or ZRANB3

To understand the role of TRF1 in telomere replication, we used SV40-immortalized conditional knockout $Trf1^{F/F}$ MEFs (Sfeir et al. 2009; Zimmermann et al. 2014). As shown before, deletion of TRF1 with Hit&Run Cre induced frequent fragile telomeres and STAs detectable in metaphase spreads (Fig. 1A,B). Previous studies revealed that TRF1 deletion leads to more frequent fragile telomere formation than BLM deletion (Sfeir et al. 2009; Zimmermann et al. 2014). We confirmed this observation by using chromosome orientation FISH (CO-FISH) to detect the leading and lagging end fragile telomeres in a side-by-side comparison of $Trf1^{F/F}$ and $Blm^{F/F}$ MEFs treated with Cre. TRF1 deletion led to extensive leading strand fragile telomere formation, which did not occur in BLM-deficient cells, and the lagging strand fragile telomeres were more frequent than in BLM-deficient cells (Supplemental Fig. S1A,B). These results further corroborate data indicating that most of the fragile telomeres induced by TRF1 loss were not due to diminished BLM recruitment (Supplemental Fig. S1A,B).

We next explored the potential pathways involved in generating the fragile telomeres in TRF1-deficient cells. To test for the involvement of BIR, we targeted the BIR factor POLD3, which diminished the fragile telomeres induced by BLM loss as previously shown (Supplemental Fig. S1C,D; Yang et al. 2020). However, POLD3 depletion did not significantly affect the fragile telomere phenotype induced by TRF1 loss as shown before (Porreca et al. 2020),

arguing against the involvement of BIR in this setting (Supplemental Fig. S1C,D). As fragile telomeres caused by RTEL1 deletion are mediated by the fork reversal factor ZRANB3 (Margalef et al. 2018), we tested whether ZRANB3 also acted at telomeres lacking TRF1. However, targeting $Zranb3$ with CRISPR/Cas9 did not change the frequency of fragile telomeres induced by TRF1 deletion (Supplemental Fig. S1E,F). These data indicate that most of the fragile telomeres in TRF1-deficient cells are independent of BIR and fork reversal by ZRANB3.

E83 in Helix2 of the TRFH domain is required for repression of telomere fragility

To determine which features of TRF1 are involved in the unexplained aspects of its role in telomere replication, we swapped domains between TRF1 and its paralog, TRF2 (Okamoto et al. 2013). Both TRF1 and TRF2 contain a charged N-terminal domain, a TRFH domain for homodimerization and protein interactions, a flexible hinge region, and a C-terminal Myb domain that binds to telomeric DNA (Fig. 1C; Broccoli et al. 1997). Swapping the TRFH domain of TRF1 for that of TRF2 (TRFHSwap mutant) failed to fully rescue the fragile telomere phenotype of TRF1-deficient cells even though the mutant was expressed and localized to telomeres (Fig. 1C–F).

The structurally similar TRFH domains of TRF1 and TRF2 are composed of 10 α helices (Fairall et al. 2001; Chen et al. 2008). Swapping of pairs of helices of the TRF2 TRFH domain into TRF1 led to mutants that were poorly expressed and/or failed to localize to telomeres (data not shown). However, the TRFHHelix2Swap mutant, in which the single Helix2 of the TRF2 TRFH domain was used to replace the corresponding helix in TRF1, was expressed well and localized to telomeres (Fig. 1C–E). This mutant elicited extensive telomere fragility similar to the TRFHSwap mutant (Fig. 1F), indicating that Helix2 is involved in the telomere replication function of TRF1.

Most of the residues of Helix2 are involved in TRFH homodimerization and thus are unlikely to be available to mediate interactions with potential effectors of TRF1 (Fig. 1C). However, E83 of mouse TRF1 is conserved in the human ortholog, and the corresponding residue in Helix2 of human and mouse TRF2 is not negatively charged (Fig. 1C). The structure of the human TRF1 TRFH domain suggests that the residue corresponding to E83 (E86) at the N-terminal end of Helix2 might be exposed and thus available for protein–protein interactions (Fig. 1C). Complementing the loss of the endogenous TRF1 with TRF1-E83K resulted in the same extensive telomere fragility observed with the TRFHSwap mutant (Fig. 1C–F). Since TRF1-E83K was expressed well and localized to telomeres (Fig. 1D,E), this result suggested that E83 is critical for the replication function of TRF1.

We next determined the effect of the E83K mutation on the ability of TRF1 to repress ATR signaling and STAs. Repression of these phenotypes correlates with the ability of TRF1 to interact with TIN2 and mediate optimal recruitment of TPP1/POT1 to telomeres (Sfeir et al. 2009). Furthermore, restoration of the TIN2/TPP1/POT1 levels at
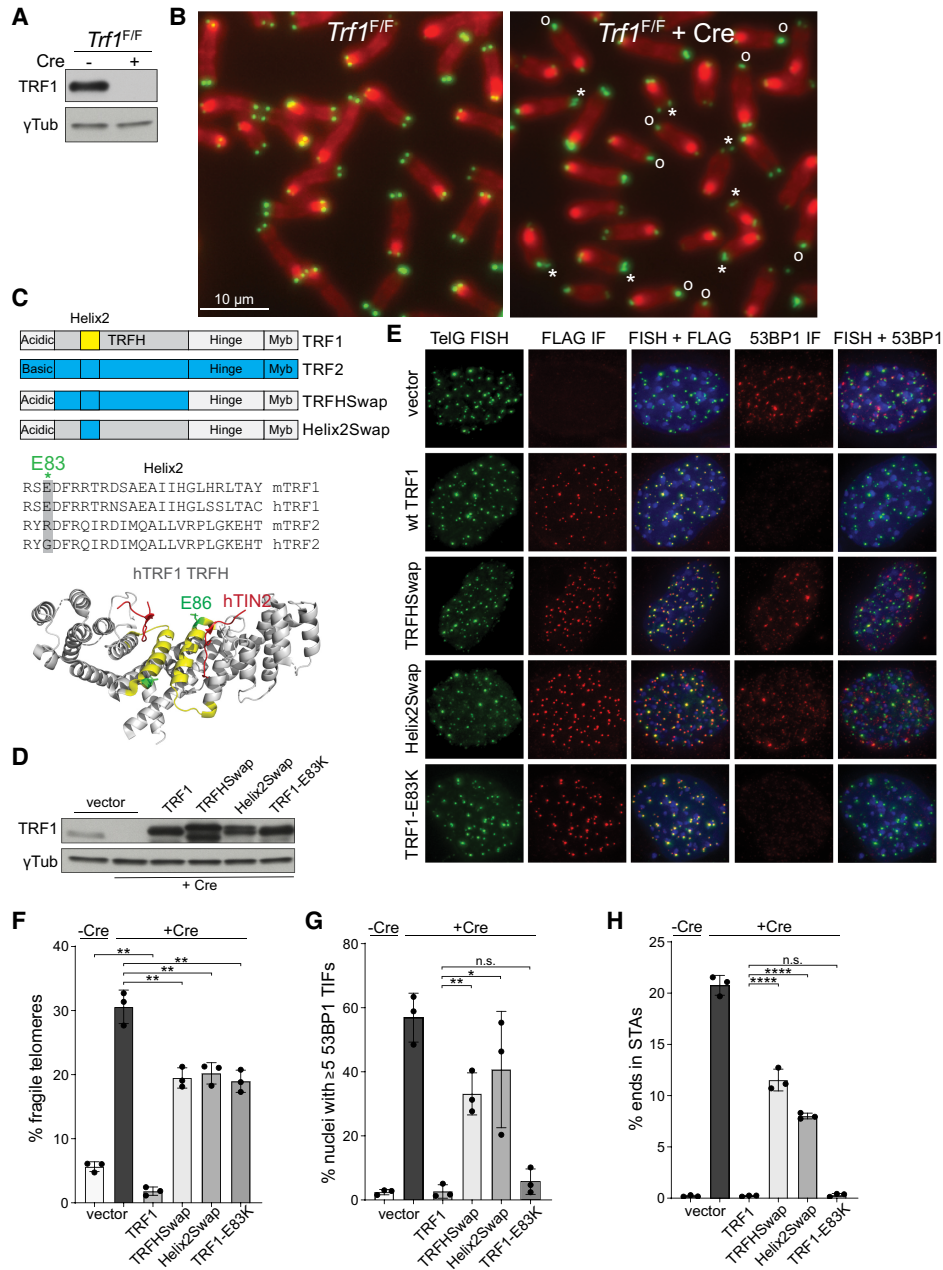
Figure 1. Helix2 of the TRF1 TRFH domain contributes to the suppression of telomere fragility. (*A*) Immunoblot analysis of TRF1 in $Trf1^{F/F}$ MEFs ± Cre (96 h). γ-Tubulin served as the loading control. (*B*) Telomere FISH on metaphase spreads of $Trf1^{F/F}$ MEFs ± Cre (96 h) with Cy3-[CCCTAA]$_3$ probes (green) and DAPI staining (red). (Asterisks) Fragile telomeres, (open circles) sister telomere associations. (*C*) Schematic representation of wild-type TRF1, TRF2, and the swapping mutants (domains are not to scale), with the Helix2 sequences in the TRF1 and TRF2 TRFH domains aligned in the *middle*, and the structure of the human TRF1 TRFH domain dimer (Chen et al. 2008) at the *bottom*. The hTIN2 peptide is in red, Helix2 is in yellow, and E86 (E83 in mice) is in green. (*D*) Immunoblot to monitor the expression of the indicated TRF1 constructs in $Trf1^{F/F}$ MEFs ± Cre (96 h). γ-Tubulin served as the loading control. (*E*) IF-FISH analysis of $Trf1^{F/F}$ MEFs + Cre (96 h) complemented with the indicated versions of TRF1 or with the vector. Telomeres were detected by FISH with Alexa 647-[TTAGGG]$_3$ probes. The TRF1 proteins were detected with anti-FLAG antibodies and Alexa 488 secondary antibodies and 53BP1 with anti-53BP1 antibodies and Alexa 555 secondary antibodies. DNA was stained with DAPI (blue). Images were false-colored for presentation purposes. (*F*) Quantification of fragile telomeres detected by FISH in $Trf1^{F/F}$ MEFs ± Cre (96 h) complemented with the corresponding constructs. Only long (q) arm telomeres were scored to avoid the confounding juxtaposition of telomeric signals at the centromeric end of the acrocentric mouse chromosomes. (*G*) Quantification of 53BP1 TIFs in $Trf1^{F/F}$ MEFs ± Cre (96 h) complemented with the indicated versions of TRF1. Data are means ± SD of three independent experiments of >50 nuclei each. (*H*) Quantification of long arm STAs detected by FISH in $Trf1^{F/F}$ MEFs ± Cre (96 h) complemented with the indicated version of TRF1. Data are means ± SD from three experiments, with ∼2000 telomeres analyzed per experiment. All *P*-values were derived from two-tailed unpaired *t*-test. (****) $P \leq 0.0001$, (**) $P \leq 0.01$, (*) $P \leq 0.05$, (n.s.) $P > 0.05$.

telomeres lacking TRF1 suppresses ATR signaling and STAs (Zimmermann et al. 2014). The POT1-mediated repression of ATR signaling is expected to be defective in cells expressing the TRFHSwap mutant because it lacks the TRF1–TIN2 interaction motif (Chen et al. 2008). In agreement with this, the TRFHSwap mutant was defective in the suppression of telomere dysfunction-induced foci (TIFs) marked by 53BP1 (Takai et al. 2003), a proxy for ATR signaling (Fig. 1E,G). The TRFHSwap mutant also failed to repress STAs (Fig. 1H). The TRFHHelix2-Swap also did not fully suppress the two phenotypes (Fig. 1E,G,H), which may be due to the proximity of Helix2 to the TIN2 interaction site (Fig. 1C; Chen et al. 2008). Importantly, the E83K point mutant was fully capable of suppressing ATR signaling and STAs (Fig. 1E,G,H). These results showed that the E83K mutant is a separation-of-function mutant that is proficient in localizing to telomeres and repressing ATR signaling and STAs while being defective in preventing fragile telomere formation.

Helix1 in the TRF1 Myb domain suppresses telomere fragility

Domain-swapping experiments also implicated the Myb domain in the replication function of TRF1. First, replacing the entire Myb domain of TRF1 with that of TRF2 (MybSwap mutant) created a version of TRF1 that failed to fully rescue the telomere fragility caused by TRF1 deletion despite its adequate expression and localization to telomeres (Fig. 2A–D). In agreement with the MybSwap mutant carrying the site where TRF1 recruits TIN2/TPP1/POT1, the MybSwap mutant suppressed ATR signaling and STAs (Fig. 2C,E,F). Similar to the MybSwap mutant, a mutant in which the Myb domain of TRF1 was replaced by the zinc finger telomeric DNA binding domain of human TZAP (TRF1-Znf9-11) (Li et al. 2017) also failed to rescue telomere fragility caused by TRF1 loss while retaining the ability to repress ATR signaling and STAs (Supplemental Fig. S2A–F). These data suggest that the Myb domain of TRF1 not only is required for its binding to telomeric DNA but has a second function in the suppression of telomere fragility.

Like all Myb domains, the TRF1 Myb domain comprises three helices: an outward-facing Helix1 and the Helix2/Helix3 pair, which form the helix–turn–helix motif that contacts the telomeric DNA (Fig. 2A; Nishikawa et al. 2001; Court et al. 2005). In some Myb domains, Helix1 can mediate protein–protein interactions (Grotewold et al. 2000; Zimmermann et al. 2004). We therefore asked whether Helix1 contributes to the ability of TRF1 to repress fragile telomere formation. Indeed, the MybHelix1-Swap mutant behaved similarly to the MybSwap mutant in that it failed to repress the fragile telomere phenotype upon TRF1 loss despite its localization at telomeres and its ability to repress ATR signaling and STAs (Fig. 2A–F). The MybHelix2Swap and MybHelix3Swap mutants also failed to suppress the fragile telomere phenotype (Fig. 2A–F). However, these mutants were expressed at a lower level and did not localize to telomeres as well as the Myb-Helix1Swap mutant, making their defect less interpretable (Fig. 2A–F).

Helix1 of the TRF1 and TRF2 Myb domains differ in a few positions, including at the LW residues at the beginning of the helix (Fig. 2A). Switching L371 and W372 in TRF1 to the corresponding residues in TRF2 resulted in a mutant (TRF1-LW-TI) that was expressed well and localized to telomeres but did not repress the fragile telomere phenotype of TRF1-deficient cells (Fig. 2A–D). The suppression of ATR signaling and STAs by TRF1-LW-TI indicated that this is a separation-of-function mutant (Fig. 2C,E,F).

The TRF1-E83K/LW-TI double mutant completely lost its ability to suppress telomere fragility (Fig. 2G). This mutant resulted in a level of fragile telomeres indistinguishable from cells not expressing TRF1 despite its proper expression and telomere localization (Fig. 2G; Supplemental Fig. S3A,B). Importantly, the double mutant retained the ability to repress ATR signaling and STAs (Supplemental Fig. S3C,D), indicating that this version of TRF1 also represents a separation-of-function mutant. The extensive fragile telomere phenotype of the E83K/LW-TI mutant suggests that Helix2 of the TRFH domain and Helix1 of the Myb domain are critical for the major mechanism by which TRF1 promotes telomere replication.

Surprisingly, the TRF1 MybSwap mutant caused rapid telomere shortening when overexpressed in wild-type MEFs (Supplemental Fig. S4). The mechanism by which the telomere shortening occurs is not known. The Myb-Helix1Swap and TRF1-LW-TI mutants only caused slight shortening of telomeres, whereas the TRF1-Znf9-11 mutant did not have a discernible effect (Supplemental Fig. S4). Therefore, it is unlikely that the extensive telomere fragility caused by these TRF1 mutants is related to the telomere shortening phenotype.

TRF1-E83K and TRF1-LW-TI cause telomere replication defects

It has been proposed that fragile telomere formation is a result of replication problems at telomeres lacking TRF1. The single-molecule analysis of the replicated DNA (SMARD) assay previously showed that TRF1 deletion leads to a reduced number of telomeric DNA molecules actively undergoing replication in a given time window (Sfeir et al. 2009), which is presumably due to transient arrest or slowdown of forks at telomeres. We therefore tested whether such replication defects occurred in cells complemented with the TRF1 separation-of-function mutants. Cells were labeled with the thymidine analog IdU for 1 h followed by a 3-h chase. This labeling protocol was repeated four times before the cells were harvested (Fig. 3A). Telomeres were then enriched based on their size after digestions of the genomic DNA with frequently cutting restriction enzymes, stretched onto silanized coverslips, and detected using telomeric FISH with a [TTAGGG]$_3$ probe combined with an anti-IdU antibody (Fig. 3A). The data confirmed that TRF1 deletion reduced the percentage of telomeres incorporating IdU by approximately twofold, consistent with prior data (Fig. 3B; Sfeir et al. 2009).
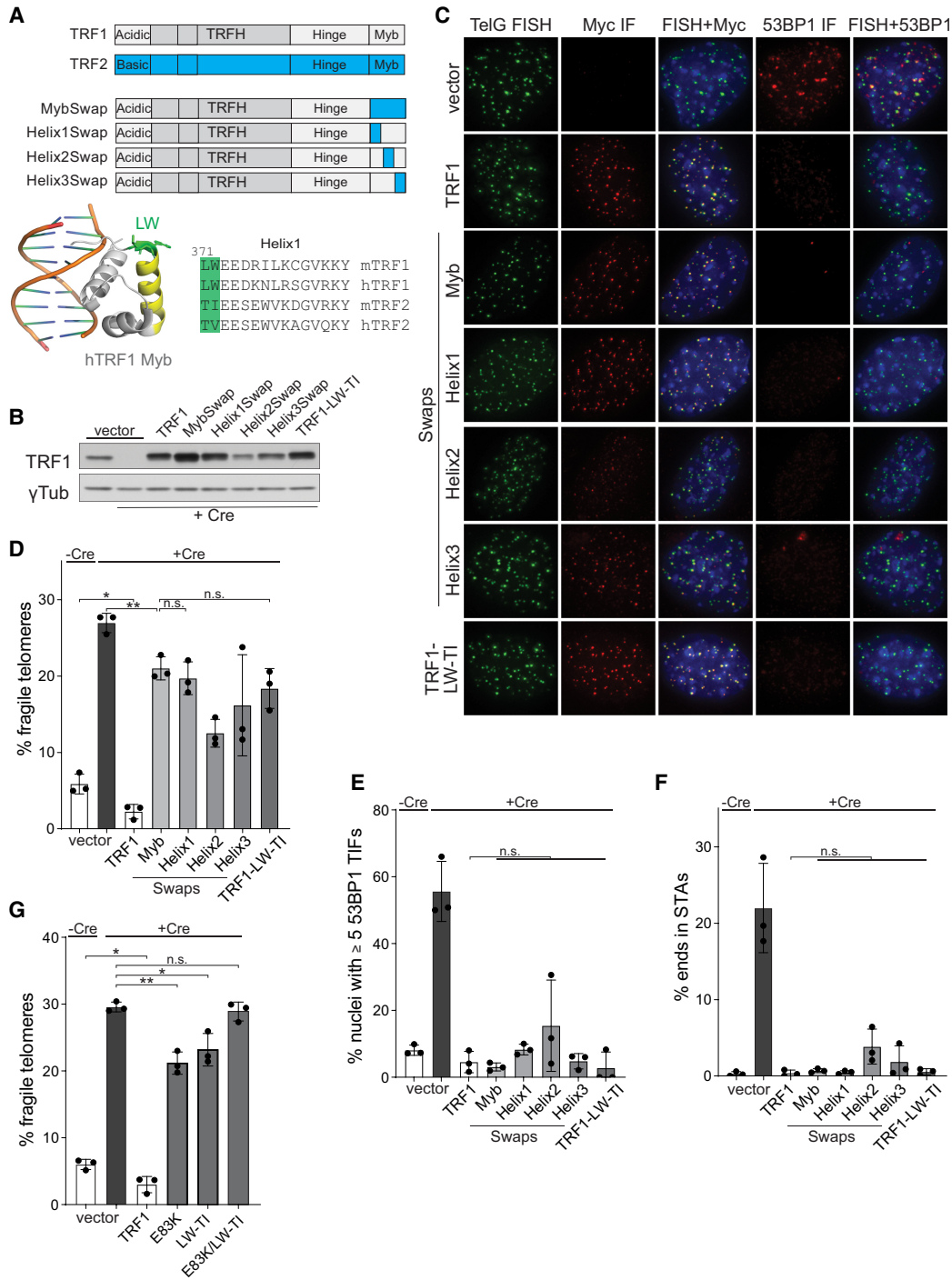
Figure 2. Helix1 of the TRF1 Myb domain contributes to the suppression of telomere fragility. (*A*) Schematic of wild-type TRF1 and TRF2 as well as the Myb-swapping mutants, with the structure of the human TRF1 Myb domain bound to telomeric DNA displayed (Court et al. 2005) *below*. Helix1 is in yellow, and LW is in green. At the *right* is an alignment of the Myb Helix1 sequence of human and mouse TRF1 and TRF2. (*B*) Immunoblot for the indicated TRF1 mutants expressed by $Trf1^{F/F}$ MEFs ± Cre (96 h). γ-Tubulin served as the loading control. (*C*) IF-FISH analysis of $Trf1^{F/F}$ MEFs + Cre (96 h) complemented with the indicated versions of TRF1. Detection of telomeric DNA, exogenous TRF1, and 53BP1 as in Figure 1E. (*D*) Quantification of fragile telomeres (as in Fig. 1D) detected by FISH in $Trf1^{F/F}$ MEFs ± Cre (96 h) complemented with the indicated versions of TRF1. (*E*) Quantification of 53BP1 TIFs (as in *C*) in $Trf1^{F/F}$ MEFs ± Cre (96 h) complemented with the indicated versions of TRF1. Data are means ± SD of three independent experiments of >50 nuclei each. (*F*) Quantification of long arm STAs detected by FISH in $Trf1^{F/F}$ MEFs ± Cre (96 h) complemented with the indicated TRF1 mutants. (*G*) Quantification of long arm fragile telomeres detected by FISH in $Trf1^{F/F}$ MEFs ± Cre (96 h) complemented with the E83K, LW-TI, and E83K/LW-TI double mutants. All metaphase analyses are means ± SD from three experiments, with ~2000 telomeres analyzed per experiment. All *P*-values were derived from two-tailed unpaired *t*-test. (**) $P \leq 0.01$, (*) $P \leq 0.05$, (n.s.) $P > 0.05$.
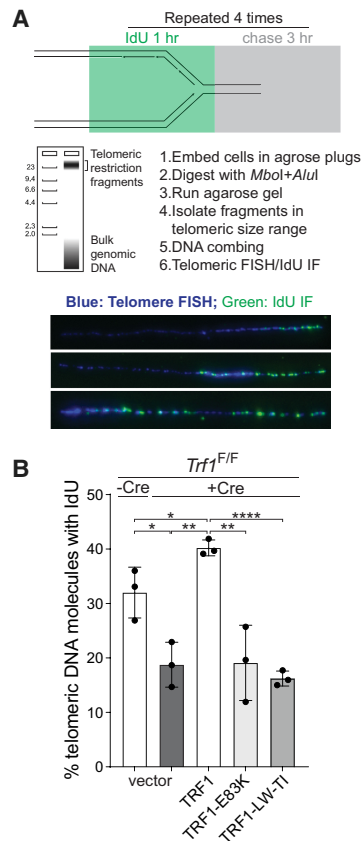
Figure 3. TRF1-E83K and TRF1-LW-TI mutants induce a telomere replication defect. (*A*) Schematic of the SMARD assay to monitor telomere replication. Examples of telomere molecules (detected by FISH) with IdU signals (detected by anti-IdU antibodies) are shown. (*B*) Quantification of telomere molecules with IdU signals by SMARD in $Trf1^{F/F}$ MEFs ± Cre (96 h) complemented with the indicated wild-type or mutant TRF1. Data are means ± SD from three experiments, with ∼100 telomere molecules analyzed per experiment. All *P*-values were derived from two-tailed unpaired *t*-test. (****) $P \leq 0.0001$, (**) $P \leq 0.01$, (*) $P \leq 0.05$.

The telomere replication defect induced by the deletion of TRF1 was rescued by exogenously expressed wild-type TRF1 (Fig. 3B). Interestingly, wild-type TRF1, which is overexpressed compared with the endogenous TRF1 (e.g., see Fig. 1D), increased the frequency of labeled telomeres compared with wild-type cells (Fig. 3B). This is consistent with the observation that such TRF1 overexpression reduced the baseline level of fragile telomeres in wild-type cells (e.g., see Figs. 1F, 2D) and suggests that the endogenous TRF1 level is insufficient to completely prevent replication problems at telomeres. TRF1-deficient cells expressing the TRF1-E83K or TRF1-LW-TI mutant showed a level of IdU incorporation at telomeres similar to cells lacking endogenous TRF1 (Fig. 3B). This result indicates that both mutants are defective in promoting efficient replication of telomeres and confirms the correlation between the fragile telomere phenotype and the replication defects. We also confirmed that the E83K

and LW-TI mutants had minimal effects on cell cycle (Supplemental Fig. S5), excluding the possibility that these mutants affected telomere replication indirectly through altering the cell cycle profile.

TFIIH is a suppressor of telomere fragility and replication defects

To identify factors that cooperate with TRF1 to promote telomere replication, we targeted a limited set of candidate genes with bulk CRISPR/Cas9 in wild-type MEFs ($Trf1^{F/F}$ not treated with Cre). The candidate genes were primarily chosen for their involvement in DNA transactions at stalled replication forks (e.g., *Brca2* and *Rad51*) or their general ability to act on DNA structures (e.g., nucleases, helicases, and DNA damage repair proteins). Each candidate gene was subjected to bulk targeting with two sgRNAs in the same transfected plasmid, and Cas9 was introduced using an adenovirus (Supplemental Fig. S6A). This strategy appeared to increase the efficacy of the knockouts, though this was not tested systematically, and the level of expression of most of the targeted factors was not determined. As a positive control, we targeted *Trf1* and *Blm*, which resulted in the same frequency of fragile telomeres as observed in MEFs lacking these genes (Supplemental Fig. S6B).

Whereas the majority of genes tested did not affect the integrity of telomeres, moderate levels of fragile telomeres were induced by knockout of several genes, including *Dhx9*, *Pif1*, and *Ascc3* (Supplemental Fig. S6B,C). DHX9 and PIF1 can unwind DNA secondary structures such as G4s and R-loops (Sanders 2010; Chakraborty and Grosse 2011), whereas ASCC3 is involved in the repair of alkylated DNA (Dango et al. 2011). How these proteins contribute to the replication of telomeric DNA remains to be determined.

We focused on two candidate genes, *Xpb* and *Xpd*, because their targeting resulted in a high frequency of fragile telomeres similar to the phenotype of TRF1 deletion (Fig. 4A–C; Supplemental Fig. S6C). In CO-FISH experiments, fragile telomeres were observed on both the leading and the lagging strand telomeres (Fig. 4B,D), as observed upon TRF1 loss. Meanwhile, no ATR signaling or STA induction was observed after *Xpb* or *Xpd* knockout (Fig. 4E,F), indicating that the telomere protection function of shelterin remained largely intact.

Apart from XPB and XPD, TFIIH also contains GTF2H1-5 and associates with the CAK complex during transcription initiation (Fig. 5A). Targeting *Gtf2h1-4* with the dual-cutting CRISPR system also led to extensive telomere fragility (Fig. 5B,C). Targeting the CAK components *Mnat1*, *Ccnh*, and *Cdk7* also induced fragile telomere formation (Fig. 5D,E). In contrast, targeting the NER factors *Xpa*, *Xpc*, *Xpf*, or *Xpg* did not affect telomere integrity (Fig. 5D,E; Supplemental Fig. S6C).

In agreement with the CRISPR targeting data, degradation of XPB induced by spironolactone (SP) (Alekseev et al. 2014) led to fragile telomere formation (Fig. 5F,G), as did inhibition of CDK7 with the specific inhibitor YKL-5-124 (CDK7i) (Fig. 5G; Olson et al. 2019). These data
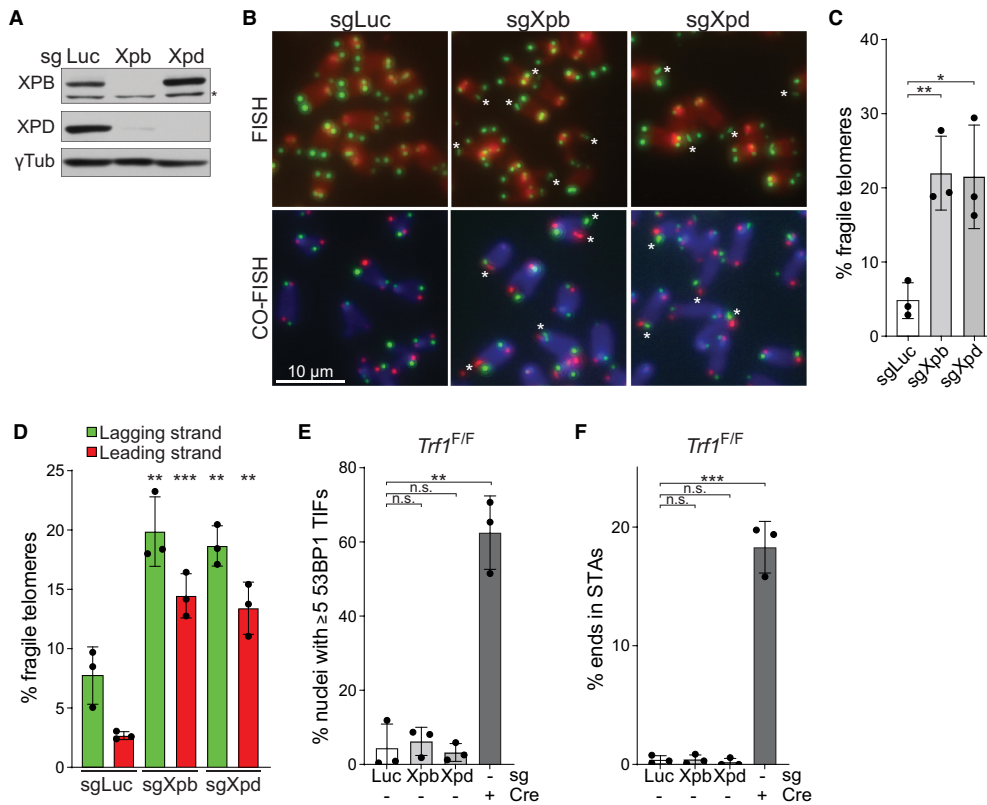
Figure 4. XPB and XPD are required for the suppression of telomere fragility. (*A*) Immunoblot for XPB and XPD to monitor expression after dual-cutting CRISPR/Cas9 targeting of the two genes (96 h). γ-Tubulin served as the loading control. (*B*) Examples of fragile telomeres caused by targeting of *Luc*, *Xpb*, or *Xpd* (96 h) detected by FISH and CO-FISH as indicated. (*C,D*) Quantification of long arm fragile telomeres detected by FISH in *C* and CO-FISH in *D* in *Trf1*$^{F/F}$ MEFs as in *B*. (*E*) Quantification of 53BP1 TIFs in *Trf1*$^{F/F}$ MEFs as in *B*. Data are means ± SD of three independent experiments of >50 nuclei each. (*F*) Quantification of long arm STAs detected by FISH in *Trf1*$^{F/F}$ MEFs as in *B*; *Trf1*$^{F/F}$ MEFs + Cre served as a positive control. All metaphase analyses are means ± SD of three experiments of ∼2000 telomeres analyzed. All *P*-values were derived from two-tailed unpaired *t*-test. (***) $P \leq 0.001$, (**) $P \leq 0.01$, (*) $P \leq 0.05$, (n.s.) $P > 0.05$.

suggest that the TFIIH holoenzyme, which includes the TFIIH core complex and the CAK subcomplex, is important for the suppression of the fragile telomere phenotype.

In the SMARD assay for telomere replication, CRISPR targeting of *Xpb* also significantly reduced the fraction of telomeric DNA molecules containing IdU (Fig. 5H). Telomeric replication was also diminished by targeting *Mnat1*, although this effect was not statistically significant (Fig. 5H).

To test whether TFIIH disruption affected genome-wide DNA replication, we examined the effect of SP and CDK7i on CFSs, which are regions where replication is challenged (Durkin and Glover 2007). CFS expression, an indicator of replication problems, can be monitored based on mitotic DNA synthesis (MiDAS) detectable on metaphase chromosomes after EdU labeling (Minocherhomji et al. 2015). As expected, inhibition of DNA replication with aphidicolin resulted in CFS expression detected based on EdU foci on metaphase chromosomes from cells incubated with EdU 1 h before harvesting (Fig. 5I,J). In contrast, SP or CDK7i did not induce CFS expression as evaluated based on MiDAS (Fig. 5I,J). In agreement, we did not observe induction of nontelomeric DNA damage foci in cells

depleted of XPB or XPD, as would be expected for cells experiencing global inhibition of DNA replication (Fig. 5K). Furthermore, unlike cells treated with aphidicolin, cells depleted of XPB or MNAT1 did not show phosphorylation of CHK1, a marker for replication stress (Fig. 5L). Therefore, it is likely that TFIIH affects replication specifically at telomeres rather than globally.

The effect of TFIIH depletion is not due to reduced TRF1 levels or telomere transcription

One straightforward explanation for the effect of TFIIH loss on telomere replication would be diminished *Trf1* gene expression due to transcriptional machinery perturbation. As expected, *Trf1*$^{F/F}$ MEFs showed an approximately twofold reduction in *Trf1* mRNA level 4 d after CRISPR targeting of *Xpb* or *Mnat1* (Supplemental Fig. S7A). However, the cells had only lost <30% of TRF1 protein, which is unlikely to account for their fragile telomere phenotype (Supplemental Fig. S7B).

To more carefully determine whether reduced *Trf1* transcription could explain the fragile telomere phenotype associated with TFIIH depletion, we monitored the
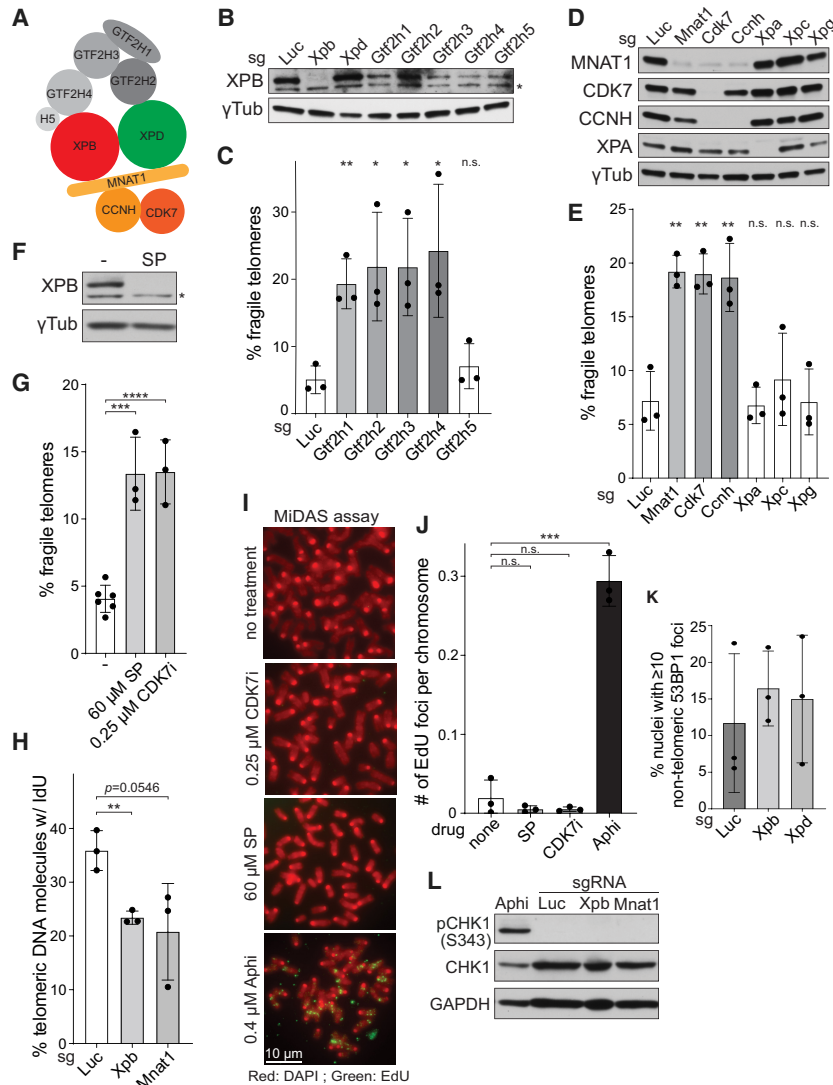
Figure 5. The TFIIH holoenzyme suppresses telomere fragility and replication defects. (*A*) Cartoon of the TFIIH holoenzyme subunits. (*B*) Immunoblot to monitor XPB levels after CRISPR/Cas9 targeting (96 h) of the indicated subunits of TFIIH. Loss of XPB confirms the knockout of the targeted genes. γ-Tubulin served as the loading control. (*C*) Quantification of long arm fragile telomeres detected by FISH in $Trf1^{F/F}$ MEFs with CRISPR/Cas9 targeting of the subunits of the TFIIH core as indicated. (*D*) Immunoblot to monitor the level of MNAT1, CDK7, CCNH, and XPA after dual-cutting CRISPR/Cas9 targeting of the corresponding genes (96 h). γ-Tubulin served as the loading control. (*E*) Quantification of long arm fragile telomeres detected by FISH in $Trf1^{F/F}$ MEFs with CRISPR/Cas9 targeting of the indicated subunits of the CAK complex or the NER proteins as in *D*. (*F*) Immunoblot to monitor the effect of 60 μM SP treatment (25 h) on XPB. γ-Tubulin served as the loading control. (*G*) Quantification of long arm fragile telomeres detected by FISH in $Trf1^{F/F}$ MEFs treated with 60 μM SP or 0.25 μM CDK7i for 25 h. (*H*) Quantification of telomere molecules with IdU signals by SMARD in $Trf1^{F/F}$ MEFs with CRISPR/Cas9 targeting of *Luc*, *Xpb*, or *Xpd* (96 h). Data are means ± SD from three experiments, with ~100 telomere molecules analyzed per experiment. (*I*) MiDAS assay to detect CFS expression. MiDAS was detected in cells treated with 10 μM EdU 1 h prior to harvesting of metaphases. $Trf1^{F/F}$ MEFs were untreated or treated with 60 μM SP, 0.25 μM CDK7i, or 0.4 μM aphidicolin for 24 h prior to EdU labeling. EdU was detected by Click chemistry (green). DNA was stained with DAPI (red). (*J*) Quantification of the number of EdU foci per chromosome in $Trf1^{F/F}$ MEFs treated with the corresponding drugs as in *I*. Data are the means ± SD of three experiments, each with 20 metaphases. (*K*) Quantification of nontelomeric 53BP1 foci in $Trf1^{F/F}$ MEFs with CRISPR/Cas9 targeting of *Luc*, *Xpb*, or *Xpd* (96 h). Data are means ± SD of three independent experiments of >50 nuclei each. (*L*) Immunoblot to monitor the level of CHK1 and phospho-CHK1 (pCHK1 S345) after CRISPR/Cas9 targeting of *Luc*, *Xpb*, or *Mnat1* with cells treated with 5 μM aphidicolin as the positive control. GAPDH served as the loading control. All metaphase analyses are means ± SD of three or more experiments of ~2000 telomeres analyzed. *P*-values were derived from two-tailed unpaired *t*-test. (****) $P \leq 0.0001$, (***) $P \leq 0.001$, (**) $P \leq 0.01$, (*) $P \leq 0.05$, (n.s.) $P > 0.05$.

TRF1 levels and the fragile telomere phenotype at different times after depletion of XPB with SP. Cells treated with SP for 20 h already showed an increase in fragile telomeres, whereas TRF1 was only reduced by 20%. At 24 and 28 h in SP, TRF1 expression was still at 70%–80%, while the fragile telomere frequency was nearly maximal (Supplemental Fig. S7C,D). That the telomere replication effect of TFIIH was independent of its role in the expression of TRF1 was further confirmed in a second MEF cell line (genotype $Trf1^{F/+}$), which for unknown reasons showed a slower dissipation of TRF1 upon SP treatment. In these cells, SP treatment for 32 h induced a threefold increase in the frequency of fragile telomeres, while there was no discernable change in the expression of TRF1 (Supplemental Fig. S7E,F).

Finally, it was previously shown that chemical inhibition of CDK7, which induces the fragile telomere phenotype (Fig. 5G), does not change global transcription program, presumably because of its redundancy with CDK12/13 (Olson et al. 2019). We therefore conclude that TFIIH affects telomere replication independently of its role in the transcription of the *Trf1* gene.

Apart from transcription of *Trf1*, we also tested the possibility that TFIIH affects telomere replication through transcription of telomeric DNA (Azzalin et al. 2007). Northern blot analysis of TERRA suggests that deletion of XPB or MNAT1 did not reduce the level of TERRA (Supplemental Fig. S8), thus arguing against this possibility. The exact function of TFIIH during telomere replication remains to be determined.

TFIIH binds TRF1 but not TRF1-E83K/LW-TI

CRISPR targeting of *Xpb* or *Xpd* in TRF1-deficient cells did not further increase the frequency of fragile telomeres (Fig. 6A,B), suggesting that TFIIH functions in the same pathway as TRF1. Therefore, we tested whether TRF1 interacts with TFIIH by coimmunoprecipitation (co-IP) with each of the subunits of the holoenzyme. Pairwise interaction analyses indicated that TRF1 interacts with XPB, GTF2H3, and GTF2H4 (Fig. 6C). These interactions were not disrupted by benzonase treatment, and TRF2 did not show interaction with these factors (Fig. 6D). Importantly, the interaction of TFIIH with TRF1 was abolished by the E83K/LW-TI mutations. These data support the idea that TRF1 promotes telomere replication by using its TRFH and Myb domains to recruit the TFIIH complex.

Interestingly, overexpression of wild-type TRF1 completely suppressed the fragile telomere phenotype induced by *Xpb* targeting, whereas TRF1-E83K/LW-TI did not (Fig. 6E,F). These results suggest that overexpression allows TRF1 to use a TFIIH-independent pathway that is not available to TRF1 when it is expressed at a physiological level. This TFIIH-independent mechanism still depends on the TRFH and Myb domains of TRF1, since overexpression of TRF1-E83K/LW-TI does not rescue the fragile telomere phenotype of *Xpb* targeting. Since the TFIIH-independent pathway is only observed upon TRF1 overexpression, we have not analyzed it further.

Discussion

The mechanism by which TRF1 ensures the replication of the duplex part of mammalian telomeres has remained a mystery for more than a decade. Here we report the unexpected role of the general transcription and NER factor TFIIH in the replication of telomeres. Depletion of TFIIH subunits led to a replication defect specific to telomeres that was comparable with the effect of TRF1 deletion. TFIIH subunits bound to TRF1, and the effect of TFIIH loss was epistatic with TRF1 deletion. Importantly, a version of TRF1 with mutations in Helix2 of its TRFH domain and Helix1 of its Myb domain (TRF1-E83K/LW-TI) was unable to interact with TFIIH, and its phenotype was identical to the telomeric phenotype of TFIIH loss. These results establish that TRF1 uses its TRFH and Myb domains to interact with subunits of TFIIH, thereby allowing TFIIH to ensure the optimal replication of telomeric DNA (Fig. 6G). Several lines of evidence indicated that the telomere replication function of TFIIH was independent of its canonical role in transcription of *Trf1*. In addition, NER factors that are not part of TFIIH did not affect telomere replication. The findings point to a noncanonical function of TFIIH in the replication of telomeres and reveal the mechanism by which TRF1 supports the progression of the replisome through the challenging telomeric TTAGGG repeat array.

Multiple mechanisms promote telomere replication

Since the discovery of fragile telomeres and fork stalling in TRF1-deficient cells (Sfeir et al. 2009), fragile telomeres have been widely used as an indicator of replication defects at telomeres, and it has become increasingly clear that fragile telomeres can be generated through multiple pathways. First, TRF1-bound BLM is thought to remove G4 structures from the lagging strand telomeric template, which when persistent create a replication gap in the lagging end telomeres (Sfeir et al. 2009; Zimmermann et al. 2014; Yang et al. 2020). When this gap is cleaved by SLX4/SLX1, the resulting DSB is repaired by BIR, which, perhaps due to the delayed lagging strand synthesis in BIR (Anand et al. 2013; Saini et al. 2013), renders the resulting telomere fragile (Yang et al. 2020). Second, TRF2 and/or PCNA-bound RTEL1 is required to resolve the telomeric t-loop structure as well as G4 obstacles to lagging strand replication (Vannier et al. 2012, 2013). The lack of t-loop resolution in the absence of RTEL1 is thought to lead to fork reversal by ZRANB3/UBC13, and the association of the reversed fork with telomerase may directly contribute to telomere fragility (Margalef et al. 2018). It is not yet understood why a telomere experiencing a reversed fork manifests itself as a fragile telomere in metaphase. Third, as shown here, the extensive telomere fragility in TRF1-deficient cells, which is independent of BIR and ZRANB3, is largely due to an important, noncanonical function of TFIIH. Both loss of TFIIH and loss of TRF1 strongly reduced incorporation of IdU in telomeric repeat arrays, directly demonstrating the telomere replication defect.

The actual molecular nature of fragile telomeres is unknown, though it is unlikely that they represent DSBs. Are there ssDNA gaps that generate uncondensed regions separating the telomeric FISH signals? Is the chromatin altered such that condensation is incomplete? Given these uncertainties of the molecular nature of the fragile telomere phenotype, the SMARD assay for telomere replication is a more reliable and robust assay to assess the role of candidate factors in telomere replication.

TRF1 protein–protein interactions

TRF1 has previously been shown to bind to tankyrase-1, tankyrase-2, TIN2, and BLM using its acidic domain, TRFH domain, and hinge region, respectively (Fig. 6G; Smith et al. 1998; Kim et al. 1999; Kaminker et al. 2001; Zimmermann et al. 2014). We identified two new protein interaction sites in TRF1: one involving Helix2 of the TRFH domain, and the other one involving Helix1 of the Myb domain (Fig. 6G). Both motifs contribute to the interaction of TRF1 with TFIIH subunits, and mutating either site results in telomere fragility and replication defects. Whereas the TRFH domain is known to support protein–protein interactions in TRF1, TRF2, and TIN2 (Chen et al. 2008; Hu et al. 2017), the finding that the Myb domain of TRF1 interacts with TFIIH was somewhat unexpected. This interaction is independent of the well-established DNA binding function of the TRF1 Myb domain, which recognizes duplex TTAGGG repeats (Nishikawa et al. 2001; Court et al. 2005). A few cases of protein–protein interactions involving plant and human Myb domains have been previously documented (Grotewold et al. 2000; Ying et al. 2000; Zimmermann et al. 2004). The Myb domain
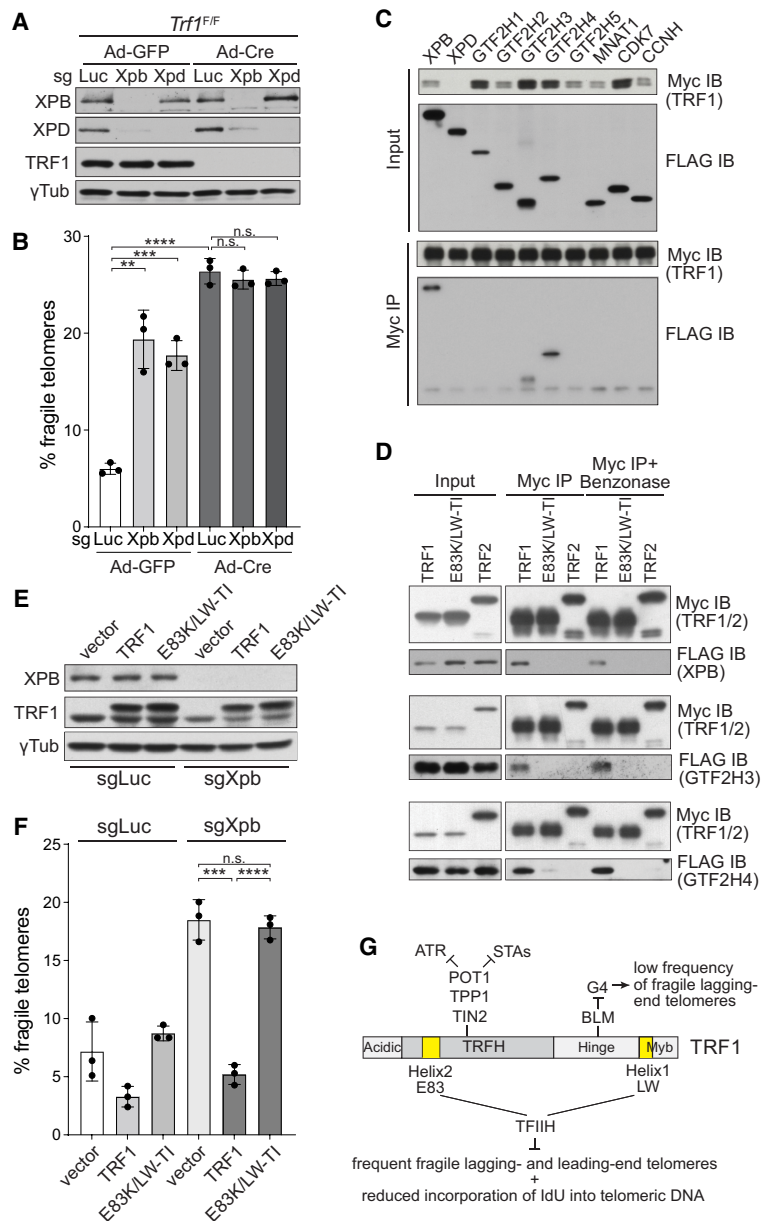
Figure 6. Epistasis and interaction of TFIIH and TRF1. (*A*) Immunoblot to monitor XPB, XPD, and TRF1 in $Trf1^{F/F}$ MEFs ± Cre (96 h) with CRISPR/Cas9 targeting of *Luc*, *Xpb*, or *Xpd* (96 h) as indicated. γ-Tubulin served as the loading control. (*B*) Quantification of long arm fragile telomeres detected by FISH in $Trf1^{F/F}$ MEFs ± Cre (96 h) with CRISPR/Cas9 targeting of *Luc*, *Xpb*, or *Xpd* (96 h) as in *A*. (*C*) Anti-Myc co-IPs of Myc-tagged mouse TRF1 and FLAG-tagged mouse TFIIH subunits from cotransfected 293FT cells. Immunoblots were probed with anti-Myc and anti-FLAG antibodies. Four percent of the lysate was run as the input. (*D*) Anti-Myc co-IPs of Myc-tagged mouse TRF1, TRF1-E83K/LW-TI, and TRF2 and FLAG-tagged mouse XPB, GTF2H3, and GTF2H4 from cotransfected 293FT cells. IP samples were treated with 25 U of benzonase where indicated. Immunoblots were probed with anti-Myc and anti-FLAG antibodies. Four percent of the lysate was run as the input. (*E*) Immunoblot to monitor XPB and TRF1 in $Trf1^{F/F}$ MEFs with overexpression of wild-type TRF1 and TRF1-E83K/LW-TI and with CRISPR/Cas9 targeting of *Luc* or *Xpb* (96 h). γ-Tubulin served as the loading control. (*F*) Quantification of long arm fragile telomeres detected by FISH in $Trf1^{F/F}$ MEFs as in *E*. All metaphase analyses are means ± SD of three experiments of ∼2000 telomeres analyzed. *P*-values were derived from two-tailed unpaired *t*-test. (****) $P \leq 0.0001$, (***) $P \leq 0.001$, (**) $P \leq 0.01$, (n.s.) $P > 0.05$. (*G*) Model of how different motifs in TRF1 function to suppress telomere fragility, replication defects, ATR signaling, and STAs.

of a meiosis-specific telomeric protein, TERB1, also has a function that is independent of its binding to DNA, presumably involving an interaction with SA3 (Shibuya et al. 2014; Zhang et al. 2017, 2022). There are two more Myb domains in shelterin: one in TRF2, which directly binds to telomeric DNA, and another one in Rap1, which has a basic surface and does not bind DNA (Hanaoka et al. 2001). It will be of interest to determine whether these Myb domains also facilitate protein–protein interactions at telomeres.

The role of the TFIIH in telomere replication

Our data implicate the TFIIH core complex in suppressing fragile telomere formation and replication defects at telomeres. In addition, the CAK subcomplex, which functions together with the TFIIH core during transcription initia-

tion, is required for this function of TFIIH. On the other hand, factors involved in NER are not required for telomere replication. While it is clear that the effect of TFIIH depletion is not simply due to diminished expression of TRF1, it remains to be determined how TFIIH participates in telomere replication. Two aspects of the TFIIH holoenzyme are of particular interest with regard to telomere replication: its DNA transaction features and its kinase activity. First, TFIIH contains two proteins that have in vitro helicase activity: the 3′-to-5′ helicase XPB and the 5′-to-3′ helicase XPD. XPB is also a DNA translocase that opens the DNA duplex in the preinitiation complex required for transcription initiation. XPB and XPD also open the DNA surrounding the lesions to create the bubble that is processed by NER. Perhaps this aspect of TFIIH is used by TRF1 to promote progression of the replisome

when it encounters unsurmountable obstacles that block the replicative helicase. It is also prudent to consider the involvement of the CAK in telomere replication. Potentially, TRF1 could use the TFIIH-tethered CAK to phosphorylate a target that affects the replication of telomeric DNA. A transcription- and NER-independent role for TFIIH in chromosome condensation was recently identified using *Xenopus* egg extracts (Haase et al. 2022). In this setting, TFIIH was proposed to promote condensin loading by removing nucleosomes or otherwise altering the chromatin environment. It is possible that chromatin alterations are also involved in the mechanism by which TFIIH facilitates the replication of the telomeric DNA.

Materials and methods

Cell culture, cloning, viral infections, and drugs

SV40-LT-immortalized $Trf1^{F/F}$ and $Blm^{F/F}$ MEFs were described previously (Chester et al. 1998; Sfeir et al. 2009; Wu et al. 2012). MEFs were cultured in DMEM (Cellgro) supplemented with 100 U/mL penicillin (Gibco), 100 µg/mL streptomycin (Gibco), 0.2 mM L-glutamine (Gibco), 0.1 mM nonessential amino acids (Gibco), and 10% bovine calf serum (HyClone). Cre recombinase was introduced by two retroviral infections with Hit&Run Cre in pMMP at 12-h intervals. Adeno-GFP (Vector Biolabs 1060) and Adeno-Cre (Vector Biolabs 1700) were used as indicated in experiments that used Adeno-Cas9. In all experiments involving Cre or Cas9, cells were harvested 120 h after the initial introduction of the virus. Mouse *Trf1* cDNA and the mutants were cloned into the pLPC-Myc-Puro or the pWZL-FLAG-Hygro vectors. MEFs infected with retroviral vectors were selected with 2.5 µg/mL puromycin or 135 µg/mL hygromycin for 3 d. shPold3 (TRCN00 00279480) and a control shLuc (CGCTGAGTACTTCGAA ATGTC) were cloned into the pLKO.1 vector. Spironolactone was purchased from Sigma (S3378), and CDK7i YKL-5-124 was from SelleckChem (S8863).

Dual-cutting Lenti-sgRNA system

sgRNAs were designed using CRISPick from the Broad Institute (https://portals.broadinstitute.org/gppx/crispick/public). For each target gene, two sgRNAs targeting spatially separate sites in the gene body were selected and cloned into the pLenti-sgRNA vector (Addgene 71409). The second sgRNA was amplified together with its U6 promoter using PCR with the following forward and reverse primers (5′ to 3′): GTGGCACCGAGTCG GTGCTTTTTTGCCCAACCCCGAGGGGACCCAGA and GC CATTTGTCTCAAGATCTAGAATTC. The amplified product was cloned into the EcoRI site of the vector containing the first sgRNA using Gibson assembly. The product containing two sgRNAs was verified by Sanger sequencing with 5′-GATAGTAG GAGGCTTGGTAGGTTTAAG-3′ as the primer. The dual-sgRNA vector was then introduced into the target cells by lentiviral infection. To initiate knockout, 2 µL of Adeno-Cas9 (Vector Biolabs 1900) was added to 200,000 cells with 8 µg/mL polybrene in 1 mL of medium in a six-well plate. Cells were replated to a 10-cm dish after 24 h and harvested after another 96 h. sgRNAs used in this study are listed in Supplemental Table S1.

Immunoblotting

Immunoblotting was performed as described (Yang et al. 2020). The following antibodies were used: mTRF1 (#1449), mTRF2 (#1254), mXPB (Bethyl Laboratories A301-337A), mXPD (CST 11963), mZRANB3 (Abclonal A9555), mPOLD3 (Proteintech 21935-1-AP), mMNAT1 (Proteintech 11719-1-AP), mCDK7 (Proteintech 27027-1-AP), mCCNH (Proteintech 67065-1-Ig), mXPA (Proteintech 16462-1-AP), mCHK1 (Santa Cruz Biotechnology sc-8408), phospho-mCHK1 S345 (CST 2348), mGAPDH (Thermo Fisher MA5-15738), and γ-Tubulin (Sigma-Aldrich GTU88).

For quantitative fluorescent immunoblotting, membranes were blocked with Intercept TBS blocking buffer (Li-Cor 927-60001) for 1 h and then incubated with primary antibodies for 2 h. After three TBST washes, membranes were incubated with fluorescently labeled secondary antibodies IRDye 800CW goat antirabbit (Li-Cor 925-32211) and IRDye 680RD goat antimouse (Li-Cor 925-68070) for 1 h, followed by three TBST washes. Imaging was performed with a GE Typhoon system and quantified using ImageJ (1.51j8).

FISH and CO-FISH

Telomere FISH on metaphase spreads was conducted as described (Celli and de Lange 2005). Briefly, cells were treated with 0.2 µg/mL colcemid for 1 h before harvesting, suspended in 0.075 M KCl, swollen for 15 min at 37°C, and fixed in 3:1 methanol:glacial acetic acid overnight. Fixed cells were dropped onto glass slides and dried overnight. Hybridization was performed with 20 nM Cy3-[CCCTAA]$_3$ PNA probes (PNA Bio) in 100 µL of hybridization mix (10 mM Tris-HCl at pH 7.2, 70% deionized formamide, 0.5% blocking reagent [Roche 11096176001]) placed onto the slides and heated for 5 min at 80°C. Slides were kept in a dark humidified chamber for 2 h, washed twice with wash buffer I (70% formamide, 10 mM Tris-HCl at pH 7.2) for 15 min each, and then washed three times for 5 min with PBS, with DAPI added to the second wash. Slides were dehydrated with 70%, 95%, and 100% ethanol before being mounted with ProLong Gold antifade reagent (Life Technologies P36934).

The procedure for telomere CO-FISH was described previously (Bailey et al. 2001; Celli et al. 2006). Briefly, cells were incubated with 7.5 µM BrdU and 2.5 µM BrdC for ~16 h before harvesting, and metaphase spreads were prepared as described above. To degrade the newly synthesized strands, slides were rehydrated with PBS, treated with 0.5 mg/mL RNase A for 15 min at 37°C, stained with 0.5 µg/mL Hoechst 33258 in 2× SSC for 15 min at room temperature, and exposed to 365-nm UV light at 5.4×10^3 J/m^2, followed by treatment with 100 µL of 10 U/µL exonuclease III (Promega M1811) for 30 min at 37°C. Slides were then washed with PBS and serially dehydrated as above. Cells were hybridized with 20 nM Cy3-[CCCTAA]$_3$ (PNA Bio) probes for 2 h at room temperature, rinsed with wash buffer I, and hybridized with 20 nM Alexa 647-[TTAGGG]$_3$ (PNA Bio) probes for 2 h at room temperature. Washing and mounting steps were as described above.

Immunofluorescence-FISH

IF-FISH was conducted as described (Takai et al. 2003). Cells were plated onto coverslips 24 h before fixation with 3% paraformaldehyde in PBS for 10 min. Coverslips were then incubated with blocking solution (0.1% BSA, 3% goat serum, 0.1% Triton X-100, 2 mM EDTA in PBS) for 30 min, followed by primary antibody incubation in blocking solution for 1 h. After three washes with PBST, cells were incubated with secondary antibodies in blocking solution for 30 min, followed by three washes with PBST. Cells were fixed again with 3% paraformaldehyde for 5 min before washing twice with PBS and dehydrating with 70%, 95%, and 100% ethanol. The FISH procedure was the same as described above, using the Alexa 488-[CCCTAA]$_3$ or Alexa 647-

[TTAGGG]₃ (PNA Bio) probes. After FISH, coverslips were washed twice with wash buffer I for 15 min each and three times with PBST, with DAPI added to the second PBST wash. Coverslips were dehydrated again before mounting onto slides. Cells were imaged using a DeltaVision microscope, and images were deconvolved. TIF analysis was done by automated focus counting as described previously (Doksani and de Lange 2016). The following antibodies were used for IF: Myc 9B11 (Cell Signaling Technologies 2276), FLAG M2 (Sigma F1804), 53BP1 (Abcam ab175933), goat antirabbit A555 (Thermo Fisher A32732), goat antimouse A647 (Thermo Fisher A21237), and goat antimouse A488 (Thermo Fisher A32723).

RT-qPCR

Total RNA was extracted with the RNeasy Plus minikit (Qiagen 74134), and first strand synthesis was carried out using the SuperScript IV first strand synthesis kit (Thermo Fisher 18091050) with random hexamers as per the manufacturer's instructions. The following primers were used for qPCR: m*Trf1* (For: CATGGACTACACAGACTTACAGC; Rev: TTCCAAGGGTGTAATACGCTC) and m*Gapdh* (For: GTGTTCCTACCCCCAATGTGT; Rev: ATTGTCATACCAGGAAATGAGCTT). qPCR was performed on a QuantStudio 12K Flex real-time PCR system (Life Technologies) at the Rockefeller University Genomics Resource Center.

FACS

For cell cycle analysis, cells were labeled with 10 μM BrdU for 30 min, fixed with cold 70% ethanol, and stored overnight. BrdU-incorporated DNA was denatured with 2 N HCl and 0.5% Triton X-100 for 30 min at room temperature. After neutralization with 0.1 M Na₂B₄O₇·10H₂O (pH 8.5), cells were incubated with FITC-conjugated anti-BrdU antibody (BD Biosciences) in PBS with 0.5% Tween 20 and 0.5% BSA for 30 min at room temperature. Cells were washed and stained with DAPI (2 mM EDTA, 0.2 mg/mL RNase A, 10 μg/mL DAPI in PBS). FACS was performed with BD LSRFortessa, and data were analyzed by FlowJo software.

Telomere restriction fragment analysis

TRF analysis was conducted as described previously (Celli and de Lange 2005). Briefly, 1 million cells were embedded in 1% agarose plugs in PBS, digested with 1 mg/mL proteinase K in digestion buffer (100 mM EDTA, 0.2% sodium deoxycholate, 1% sodium lauryl sarcosine), and washed extensively in TE buffer (10 mM Tris at pH 8, 1 mM EDTA). The DNA in the plugs was digested with 60 U of AluI and MboI overnight. Plugs were run on a 1% agarose gel using pulse field gel electrophoresis, and the gel was dried. ³²P-γ-ATP-labeled TelC probes ([CCCTAA]₄) were used for probing telomeric overhang under native conditions. After washing and imaging, the gel was denatured, reprobed, and imaged again. Imaging was performed with a GE Typhoon system.

Coimmunoprecipitation

Three million 293FT cells were plated and, 24 h later, 10 μg of each plasmid was transfected into the cells using calcium-phosphate coprecipitation. Medium was refreshed 12 h later. Cells were harvest 48 h after transfection and snap-frozen. Cell pellets were lysed in 250 μL of lysis buffer (40 mM HEPES at pH 7.5, 150 mM NaCl, 10% glycerol, 1 mM EDTA, 0.5% CHAPS, 1% Triton X-100, supplemented with protease inhibitors [Roche]) for 30 min, followed by centrifugation. Aliquots of the supernatants were saved as input samples, and 1 μL of anti-Myc antibodies

(Cell Signaling 2276) was used for each IP. Samples were incubated on a nutator for 2 h at 4°C, followed by 1-h incubation with magnetic protein G beads (CST 9006S). The beads were washed three times with the lysis buffer, and bound proteins were eluted with Laemmli buffer for analysis on SDS/PAGE gels.

Northern blot

Northern blot for detection of TERRA was adapted from a previous study (Azzalin et al. 2007). Briefly, total RNA was extracted using TRIzol. Five micrograms of RNA was run on a 1.2% agarose gel in FA buffer (20 mM MOPS at pH 7.0, 5 mM sodium acetate, 1 mM EDTA, 0.67% formaldehyde). After electrophoresis, the gel was soaked in 0.05 M NaOH and 1.5 M NaCl for 10 min and then in 10× SSC for 15 min. The RNA was then transferred onto a nylon N⁺ membrane and cross-linked by UV. The membrane was blocked in Church buffer (50% sodium phosphate buffer [0.684 M Na₂HPO₄, 0.316 M NaH₂PO₄ at pH 7.2], 1 mM EDTA, 7% SDS, 1% BSA) for 90 min at 55°C followed by hybridization overnight at 60°C with ³²P-γ-ATP-labeled TelC probes ([CCCTAA]₄). The membrane was then washed twice with 2× SSC and 0.2% SDS and once with 0.5× SSC and 0.2% SDS at 55°C, and finally exposed to a PhosphorImager screen and scanned using the GE Typhoon system.

SMARD

The SMARD assay was adapted from previous studies (Norio and Schildkraut 2001; Sfeir et al. 2009). Cells (2.5 million) were plated 16 h before labeling. The next day, cells were labeled with 25 μM IdU for 1 h followed by three washes with PBS and then incubated with fresh medium for 3 h (chase). The process was repeated and, after the fourth labeling, cells were washed with PBS and harvested. The cell pellets were embedded in 1% low-melt agarose plugs and treated with 1 mg/mL Proteinase K overnight at 50°C followed by extensive washes with TE. The plugs were then digested with 60 U of AluI and MboI overnight at 37°C. The next day, plugs were run on a 1% low-melt agarose gel in TAE buffer alongside a λ DNA MW marker at 90 V for 30 min. A slice above the 23-kb λ marker was excised and transferred to a 15-mL falcon tube, and 2 mL of buffer (35 mM MES hydrate, 15 mM MES sodium salt, titrated to pH 5.4 with HCl) was added. The samples were heated for 20 min at 68°C to melt the agarose and transferred to 42°C. After 10 min, 20 μL of β-Agarase I (NEB M0392S) was added, and the samples were kept overnight at 42°C. The next day, the DNA samples were stretched onto silanized coverslips using the FiberComb system (Genomic Vision), after which the coverslips were dried for 2 h at 68°C. For telomere staining, coverslips were first denatured in the alkaline-denaturing buffer (0.1 N NaOH in 70% ethanol, 0.1% β-mercaptoethanol) for 15 min, fixed in 0.5% glutaraldehyde for 5 min, and serially dehydrated with ethanol. Coverslips were hybridized to Cy3-[TTAGGG]₃ PNA probes (PNA Bio) for 2 h in hybridization mix as in metaphase FISH, washed twice for 15 min with hybridization wash I (70% formamide, 10 mM Tris-HCl at pH 7.2), and washed twice for 5 min with PBS. For IdU staining, coverslips were blocked with 5% BSA in PBS for 1 h. Anti-IdU antibody (Abcam ab6326) was added with the blocking solution and incubated overnight. Last, coverslips were washed three times with PBS and incubated with the Alexa 488 donkey antirat secondary antibody (Thermo Fisher 21208), followed by PBS washes and mounting with ProLong Gold antifade reagent (Life Technologies P36934).

MiDAS assay

Cells were treated with 60 µM SP, 0.25 µM CDK7i, or 0.4 µM aphidicolin for 24 h and then incubated with 10 mM EdU and 0.2 µg/mL colcemid for 1 h. Cells were harvested and dropped as in metaphase FISH. EdU staining was performed using the Click-iT EdU Alexa fluor 647 kit (Invitrogen C10340) as per the manufacturer's instructions.

Statistics and reproducibility

Data sets were analyzed using GraphPad Prism 9, and differences between samples were determined using a two-tailed, unpaired t-test unless otherwise stated. Error bars represent standard deviation. Significance levels are given as follows: $P \leq 0.0001$ (****), $P \leq 0.001$ (***), $P \leq 0.01$ (**), $P \leq 0.05$ (*), and $P > 0.05$ (n.s. [not significant]). Experiments were repeated at least three times.

Data availability

All data supporting the findings of this study are available here and in the Supplemental Material.

Competing interest statement

T.d.L. is a member of the Scientific Advisory Board of Calico, LLC.

Acknowledgments

References

Alekseev S, Ayadi M, Brino L, Egly J-M, Larsen AK, Coin F. 2014. A small molecule screen identifies an inhibitor of DNA repair inducing the degradation of TFIIH and the chemosensitization of tumor cells to platinum. *Chem Biol* **21:** 398–407. doi:10.1016/j.chembiol.2013.12.014

Anand RP, Lovett ST, Haber JE. 2013. Break-induced DNA replication. *Cold Spring Harb Perspect Biol* **5:** a010397. doi:10.1101/cshperspect.a010397

Azzalin CM, Reichenbach P, Khoriauli L, Giulotto E, Lingner J. 2007. Telomeric repeat-containing RNA and RNA surveillance factors at mammalian chromosome ends. *Science* **318:** 798–801. doi:10.1126/science.1147182

Bailey SM, Cornforth MN, Kurimasa A, Chen DJ, Goodwin EH. 2001. Strand-specific postreplicative processing of mammalian telomeres. *Science* **293:** 2462–2465. doi:10.1126/science.1062560

Broccoli D, Smogorzewska A, Chong L, de Lange T. 1997. Human telomeres contain two distinct Myb–related proteins, TRF1 and TRF2. *Nat Genet* **17:** 231–235. doi:10.1038/ng1097-231

Celli GB, de Lange T. 2005. DNA processing is not required for ATM-mediated telomere damage response after TRF2 deletion. *Nat Cell Biol* **7:** 712–718. doi:10.1038/ncb1275

Celli GB, Denchi EL, de Lange T. 2006. Ku70 stimulates fusion of dysfunctional telomeres yet protects chromosome ends from homologous recombination. *Nat Cell Biol* **8:** 885–890. doi:10.1038/ncb1444

Chakraborty P, Grosse F. 2011. Human DHX9 helicase preferentially unwinds RNA-containing displacement loops (R-loops) and G-quadruplexes. *DNA Repair* **10:** 654–665. doi:10.1016/j.dnarep.2011.04.013

Chen Y, Yang Y, van Overbeek M, Donigian JR, Baciu P, de Lange T, Lei M. 2008. A shared docking motif in TRF1 and TRF2 used for differential recruitment of telomeric proteins. *Science* **319:** 1092–1096. doi:10.1126/science.1151804

Chester N, Kuo F, Kozak C, O'Hara CD, Leder P. 1998. Stage-specific apoptosis, developmental delay, and embryonic lethality in mice homozygous for a targeted disruption in the murine Bloom's syndrome gene. *Genes Dev* **12:** 3382–3393. doi:10.1101/gad.12.21.3382

Compe E, Egly JM. 2016. Nucleotide excision repair and transcriptional regulation: TFIIH and beyond. *Annu Rev Biochem* **85:** 265–290. doi:10.1146/annurev-biochem-060815-014857

Court R, Chapman L, Fairall L, Rhodes D. 2005. How the human telomeric proteins TRF1 and TRF2 recognize telomeric DNA: a view from high-resolution crystal structures. *EMBO Rep* **6:** 39–45. doi:10.1038/sj.embor.7400314

Dango S, Mosammaparast N, Sowa ME, Xiong LJ, Wu F, Park K, Rubin M, Gygi S, Harper JW, Shi Y. 2011. DNA unwinding by ASCC3 helicase is coupled to ALKBH3-dependent DNA alkylation repair and cancer cell proliferation. *Mol Cell* **44:** 373–384. doi:10.1016/j.molcel.2011.08.039

de Lange T. 2018. Shelterin-mediated telomere protection. *Annu Rev Genet* **52:** 223–247. doi:10.1146/annurev-genet-032918-021921

Doksani Y, de Lange T. 2016. Telomere-internal double-strand breaks are repaired by homologous recombination and PARP1/Lig3-dependent end-joining. *Cell Rep* **17:** 1646–1656. doi:10.1016/j.celrep.2016.10.008

Durkin SG, Glover TW. 2007. Chromosome fragile sites. *Annu Rev Genet* **41:** 169–192. doi:10.1146/annurev.genet.41.042007.165900

Fairall L, Chapman L, Moss H, de Lange T, Rhodes D. 2001. Structure of the TRFH dimerization domain of the human telomeric proteins TRF1 and TRF2. *Mol Cell* **8:** 351–361. doi:10.1016/S1097-2765(01)00321-5

Grotewold E, Sainz MB, Tagliani L, Hernandez JM, Bowen B, Chandler VL. 2000. Identification of the residues in the Myb domain of maize C1 that specify the interaction with the bHLH cofactor R. *Proc Natl Acad Sci* **97:** 13579–13584. doi:10.1073/pnas.250379897

Haase J, Chen R, Parker WM, Bonner MK, Jenkins LM, Kelly AE. 2022. The TFIIH complex is required to establish and maintain mitotic chromosome structure. *Elife* **11:** 1–25. doi:10.7554/eLife.75475

Hanaoka S, Nagadoi A, Yoshimura S, Aimoto S, Li B, De Lange T, Nishimura Y. 2001. NMR structure of the hRap1 Myb motif reveals a canonical three-helix bundle lacking the positive surface charge typical of Myb DNA-binding domains. *J Mol Biol* **312:** 167–175. doi:10.1006/jmbi.2001.4924

Hockemeyer D, Collins K. 2015. Control of telomerase action at human telomeres. *Nat Struct Mol Biol* **22:** 848–852. doi:10.1038/nsmb.3083

Hu C, Rai R, Huang C, Broton C, Long J, Xu Y, Xue J, Lei M, Chang S, Chen Y. 2017. Structural and functional analyses of the

mammalian TIN2–TPP1–TRF2 telomeric complex. *Cell Res* 27: 1485–1502. doi:10.1038/cr.2017.144

Kaminker PG, Kim SH, Taylor RD, Zebarjadian Y, Funk WD, Morin GB, Yaswen P, Campisi J. 2001. TANK2, a new TRF1-associated poly(ADP-ribose) polymerase, causes rapid induction of cell death upon overexpression. *J Biol Chem* 276: 35891–35899. doi:10.1074/jbc.M105968200

Kim SH, Kaminker P, Campisi J. 1999. TIN2, a new regulator of telomere length in human cells. *Nat Genet* 23: 405–412. doi:10.1038/70508

Li JSZ, Miralles Fusté J, Simavorian T, Bartocci C, Tsai J, Karlseder J, Lazzerini Denchi E. 2017. TZAP: a telomere-associated protein involved in telomere length control. *Science* 355: 638–641. doi:10.1126/science.aah6752

Margalef P, Kotsantis P, Borel V, Bellelli R, Panier S, Boulton SJ. 2018. Stabilization of reversed replication forks by telomerase drives telomere catastrophe. *Cell* 172: 439–453.e14. doi:10.1016/j.cell.2017.11.047

Martínez P, Thanasoula M, Muñoz P, Liao C, Tejera A, McNees C, Flores JM, Fernández-Capetillo O, Tarsounas M, Blasco MA. 2009. Increased telomere fragility and fusions resulting from *TRF1* deficiency lead to degenerative pathologies and increased cancer in mice. *Genes Dev* 23: 2060–2075. doi:10.1101/gad.543509

Minocherhomji S, Ying S, Bjerregaard VA, Bursomanno S, Aleliunaite A, Wu W, Mankouri HW, Shen H, Liu Y, Hickson ID. 2015. Replication stress activates DNA repair synthesis in mitosis. *Nature* 528: 286–290. doi:10.1038/nature16139

Nishikawa T, Okamura H, Nagadoi A, König P, Rhodes D, Nishimura Y. 2001. Solution structure of a telomeric DNA complex of human TRF1. *Structure* 9: 1237–1251. doi:10.1016/S0969-2126(01)00688-8

Norio P, Schildkraut CL. 2001. Visualization of DNA replication on individual Epstein–Barr virus episomes. *Science* 294: 2361–2364. doi:10.1126/science.1064603

Okamoto K, Bartocci C, Ouzounov I, Diedrich JK, Yates JR, Denchi EL. 2013. A two-step mechanism for TRF2-mediated chromosome-end protection. *Nature* 494: 502–505. doi:10.1038/nature11873

Olson CM, Liang Y, Leggett A, Park WD, Li L, Mills CE, Elsarrag SZ, Ficarro SB, Zhang T, Düster R, et al. 2019. Development of a selective CDK7 covalent inhibitor reveals predominant cell-cycle phenotype. *Cell Chem Biol* 26: 792–803.e10. doi:10.1016/j.chembiol.2019.02.012

Porreca RM, Herrera-Moyano E, Skourti E, Law PP, Gonzalez Franco R, Montoya A, Faull P, Kramer H, Vannier J-B. 2020. TRF1 averts chromatin remodelling, recombination and replication dependent-break induced replication at mouse telomeres. *Elife* 9: 1–28. doi:10.7554/eLife.49817

Saini N, Ramakrishnan S, Elango R, Ayyar S, Zhang Y, Deem A, Ira G, Haber JE, Lobachev KS, Malkova A. 2013. Migrating bubble during break-induced replication drives conservative DNA synthesis. *Nature* 502: 389–392. doi:10.1038/nature12584

Sanders CM. 2010. Human Pif1 helicase is a G-quadruplex DNA-binding protein with G-quadruplex DNA-unwinding activity. *Biochem J* 430: 119–128. doi:10.1042/BJ20100612

Schier AC, Taatjes DJ. 2020. Structure and mechanism of the RNA polymerase II transcription machinery. *Genes Dev* 34: 465–488. doi:10.1101/gad.335679.119

Sfeir A, Kosiyatrakul ST, Hockemeyer D, MacRae SL, Karlseder J, Schildkraut CL, de Lange T. 2009. Mammalian telomeres resemble fragile sites and require TRF1 for efficient replication. *Cell* 138: 90–103. doi:10.1016/j.cell.2009.06.021

Shibuya H, Ishiguro K, Watanabe Y. 2014. The TRF1-binding protein TERB1 promotes chromosome movement and telomere rigidity in meiosis. *Nat Cell Biol* 16: 145–156. doi:10.1038/ncb2896

Smith S, Giriat I, Schmitt A, de Lange T. 1998. Tankyrase, a poly (ADP-ribose) polymerase at human telomeres. *Science* 282: 1484–1487. doi:10.1126/science.282.5393.1484

Takai H, Smogorzewska A, de Lange T. 2003. DNA damage foci at dysfunctional telomeres. *Curr Biol* 13: 1549–1556. doi:10.1016/S0960-9822(03)00542-6

Vannier J-B, Pavicic-Kaltenbrunner V, Petalcorin MIR, Ding H, Boulton SJ. 2012. RTEL1 dismantles T loops and counteracts telomeric G4-DNA to maintain telomere integrity. *Cell* 149: 795–806. doi:10.1016/j.cell.2012.03.030

Vannier J-B, Sandhu S, Petalcorin MIR, Wu X, Nabi Z, Ding H, Boulton SJ. 2013. RTEL1 is a replisome-associated helicase that promotes telomere and genome-wide replication. *Science* 342: 239–242. doi:10.1126/science.1241779

Wu P, Takai H, De Lange T. 2012. Telomeric 3′ overhangs derive from resection by Exo1 and apollo and fill-in by POT1b-associated CST. *Cell* 150: 39–52. doi:10.1016/j.cell.2012.05.026

Yang Z, Takai KK, Lovejoy CA, de Lange T. 2020. Break-induced replication promotes fragile telomere formation. *Genes Dev* 34: 1392–1405. doi:10.1101/gad.328575.119

Ying GG, Proost P, Van Damme J, Bruschi M, Introna M, Golay J. 2000. Nucleolin, a novel partner for the Myb transcription factor family that regulates their activity. *J Biol Chem* 275: 4152–4158. doi:10.1074/jbc.275.6.4152

Zhang J, Tu Z, Watanabe Y, Shibuya H. 2017. Distinct TERB1 domains regulate different protein interactions in meiotic telomere movement. *Cell Rep* 21: 1715–1726. doi:10.1016/j.celrep.2017.10.061

Zhang K, Tarczykowska A, Gupta DK, Pendlebury DF, Zuckerman C, Nandakumar J, Shibuya H. 2022. The TERB1 MYB domain suppresses telomere erosion in meiotic prophase I. *Cell Rep* 38: 110289. doi:10.1016/j.celrep.2021.110289

Zimmermann IM, Heim MA, Weisshaar B, Uhrig JF. 2004. Comprehensive identification of *Arabidopsis thaliana* MYB transcription factors interacting with R/B-like BHLH proteins. *Plant J* 40: 22–34. doi:10.1111/j.1365-313X.2004.02183.x

Zimmermann M, Kibe T, Kabir S, de Lange T. 2014. TRF1 negotiates TTAGGG repeat-associated replication problems by recruiting the BLM helicase and the TPP1/POT1 repressor of ATR signaling. *Genes Dev* 28: 2477–2491. doi:10.1101/gad.251611.114